Journal of Luminescence 132 (2012) 659–664

Contents lists available at SciVerse ScienceDirect

Journal of Luminescence

journal homepage: www.elsevier.com/locate/jlumin

Blue and red dual emission nanophosphor $CaMgSi_2O_6:Eu^{n+}$; crystal structure and electronic configuration

A.U. Pawar [a], Abhijit P. Jadhav [a], U. Pal [b], Byung Kyu Kim [c], Young Soo Kang [a,*]

[a] Department of Chemistry, Sogang University, #1 Shinsu- dong, Mapo-gu, Seoul 121-742, Korea
[b] Instituto de Fisica Benemerita, Universidad Autonoma de Puebla, Apodo. Postal J-48, Puebla, Pue 72570, Mexico
[c] Department of Polymer Science and Engineering, Pusan National University, Busan 609-735, Korea

ARTICLE INFO

Article history:
Received 27 June 2011
Accepted 29 September 2011
Available online 12 October 2011

Keywords:
Dual emission
Solvent effect
$CaMgSi_2O_6:Eu^{n+}$
Crystal structure

ABSTRACT

Well dispersed Eu doped $CaMgSi_2O_6$ (CMS) nanoparticles of 12–19 nm average sizes were synthesized by the co-precipitation method using different ratios of water and ethanol mixture as a solvent and subsequent air annealing. While ethanol as solvent produced pure CMS in monoclinic phase, pure water produced $Ca_2MgSi_2O_7$ (C2MS) and CMS in the mixed phase. Apart from the composition of CMS and C2MS, concentration and ionization state of the activator depended strongly on the composition (effective dielectric constant) of the solvent. Both the blue and red emission bands could be revealed for the europium activated CMS nanoparticles using single europium precursor. Efficiency of blue and red emissions in the nanophosphors, controlled by the relative abundance of europium in Eu^{2+} and Eu^{3+} oxidation states, could be controlled by adjusting the water content in the solvent. The relative intensity of the red emission (615 nm) decreased with the increase of water content in the solvent.

1. Introduction

Phosphor materials are widely used in various application such as fluorescent lamps, cathode ray tubes, vacuum fluorescent display, plasma display, LED, polyhouses etc [1,2]. Different types of phosphors with blue, red, green, and sometimes with dual emission characteristics are required for technological applications. Generally, these phosphor materials are the activator (dopant) incorporated host matrices like oxides, sulfides, garnets, vanadates and oxysulfides of metals. $CaMgSi_2O_6$ (CMS) is a well known host material, which is a major pyroxene mineral (diopside) of peridotites, basalts, and an important constituent of the mantle, which has been studied by many researchers [3–6]. On the other hand, CMS is a good bio-compatible materials with high bioactivity [7–9], high thermal stability [10,11], and the sintered diopside form seems to form bonds with living bone tissues more rapidly than apatite [9,12,13].

In agricultural crops, wavelength conversion efficiency assists photosynthetic process. Plants, algae and some bacteria use solar energy to synthesize sugar and other life-essential compounds [14,15]. They harvest sunlight primarily through the chlorophyll antenna with accessory carotenes and xanthophylls with near perfect transformation efficiency. However, these compounds only absorb blue and red light, leading to other parts of sunlight unused [16–18]. To improve the photosynthesis process i.e. light conversion efficiency, it is necessary to convert the unused portion of sunlight into blue and red light. Red and blue dual emission behavior of Cu^+ and Eu^{2+} activated phosphors (dual-excitation, dual-emission phosphors) on ultraviolet (UV) and visible excitations has been reported by Lian et al. [19] On the other hand, light wavelength conversion of both ultraviolet (from 245 to 415 nm) and visible region (from 415 to 595 nm) by praseodymium complexes with aromatic carboxylic acids has been demonstrated by Yan et al. [20] Dual emission has also been reported in fluorescent dye system and rare earth doped organic complexes [21–27]. CMS is a well known phosphor material with the possibility of emitting light in the blue and red spectral regions. Jiang et al. [28] have prepared Eu^{2+}, Dy^{3+} and Nd^{3+} activated CMS, with intense blue emission under UV illumination. Daud et al. [29] have reported the synthesis of blue and red emitting europium activated CMS phosphors using EuF_3 and Eu_2O_3 as Eu precursors, respectively. However, the fabrication of CMS nanophosphors with dual (blue and red) emission through single excitation energy has not been reported yet.

In the present study, we describe the synthesis of Eu doped CMS nanoparticles through simple chemical co-precipitation technique. Eu^{2+} and Eu^{3+} ionization states of the activator, responsible for dual emission in the CMS host have been controlled through the variation of solvent composition in the co-precipitation process using single dopant precursor. Role of solvent composition on the crystal structure and dual emission behavior of the europium doped CMS nanoparticles have been discussed.

* Corresponding author. Tel.: +82 2 705 8882.
E-mail address: yskang@sogang.ac.kr (Y.S. Kang).

0022-2313/$ - see front matter © 2011 Elsevier B.V. All rights reserved.
doi:10.1016/j.jlumin.2011.09.058

2. Experimental

2.1. Materials

Calcium chloride ($CaCl_2$, 95.0%, Junsei Chemicals Co. Ltd.), magnesium chloride ($MgCl_2$, extra pure, Junsei Chemicals Co. Ltd.), tetraethylorthosilicate, ($(C_2H_5O)_4Si$, TEOS, 98.0%, Samchung Chemicals), europium(III) chloride hexahydrate, ($EuCl_3 \cdot 6H_2O$, 99.9% metal basis, Aldrich), ammonia water, (NH_4OH, extra pure, Jin Chemical Pharmaceutical Co. Ltd.), ethyl alcohol, (C_2H_5OH, 94.0%, Samchung Chemicals) were used as received without further purification.

2.2. Synthesis

Synthesis of europium doped $CaMgSi_2O_6$ nanoparticles was carried out through chemical co-precipitation. For that, 0.015 mol of $CaCl_2$ (0.4162 g), 0.015 mol of $MgCl_2$ (0.3570 g), 0.030 mol of TEOS (1.6728 mL) and 0.0015 mol $EuCl_3 \cdot 6H_2O$ (0.1373 g) were dissolved in a 250 mL of water–ethanol mixture solvent. The volumetric ratios of water and ethanol in the mixed solvent were maintained as either 1:0, 1:1 or 0:1. After stirring the mixture vigorously for 1 h, 10 mL of NH_4OH solution (28–30%) was added to the reaction mixture. On adding the NH_3 solution, the color of the reaction mixture turned white. The white mixture solution was kept at room temperature under magnetic stirring for another 8 h. Finally the precipitate was separated from the mixture solution by centrifugation and washed several times using deionized (DI) water. The obtained product was dried at 120 °C, and calcinated at 1100 °C for 2 h in air ambient.

2.3. Characterizations

For structure determination, powder X-ray diffraction (XRD) patterns of the samples were recorded using the CuKα radiation (λ=1.5406 Å) of a Rigaku X-ray diffractometer. Surface morphology and elemental composition of the as-synthesized and annealed samples were studied with the use of a field emission scanning electron microscope (FE-SEM, JEOL LTD JSM 890). A field emission JEOL JEM 2100F transmission electron microscope (TEM), operating at 200 kV was utilized to determine the size, shape and crystallinity of the synthesized CMS and C2MS nanophosphors. Room temperature photoluminescence (PL) emissions of the powder samples were measured with the help of a Hitachi F-7000 fluorescence spectrophotometer using the 337 nm excitation of a Xenon lamp. A Thermo VG Scientific (England), Multitab 2000 X-ray photoelectron spectrometer (XPS) was used to estimate the surface elemental composition and chemical state of the elements in the samples. To determine the valence state of the activator Eu in host matrix, electron spin resonance (ESR) spectra of the samples were recorded in an X-band JEOL JEX-FX 200–300 analyzer, using a microwave frequency of 9.18 GHz, microwave power of 0.99 mW, and modulation field of 100 Hz. Room temperature CL spectra was measured on Low Vacuum Scanning Electron Microscope (JEOL Japan, JSM-6490 LV Gatan (U.K) mono CL3+).

3. Results and discussion

Fig. 1 shows the XRD patterns of the CMS samples prepared with different volume ratios of water and ethanol. While the sample prepared with ethanol as a solvent (W:E=0:1) revealed diffraction peaks related to monoclinic CMS phase (JCPDS # 01–070-3482) with low intense peaks of $Ca_2MgSi_2O_7$ (C2MS) phase (JCPDS# 01–074-0990). When the water quantity of the solvent increased (i.e. W:E=1:1) revealed diffraction peaks correspond to both CMS and $Ca_2MgSi_2O_7$ (C2MS) phases with equal intensity. The

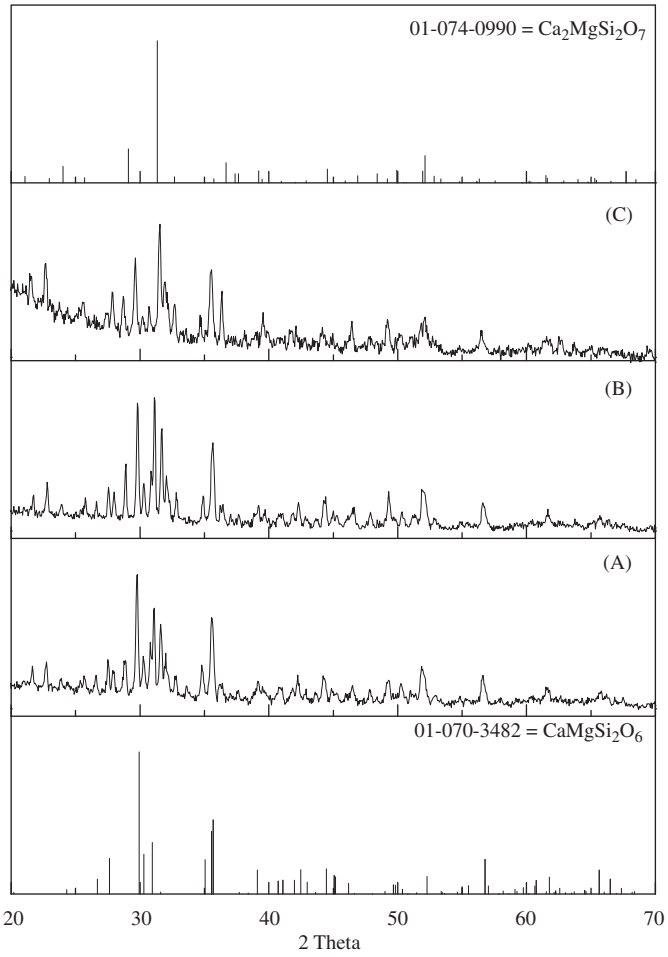

Fig. 1. Comparative XRD spectra of the CMS nanophosphors synthesized using solvents with water–ethanol volume ratio (A) 0:1, (B) 1:1 and (C) 1:0. All the samples were calcinated at 1100 °C for 2 h in air.

sample prepared with pure water (W:E=1:0) showed diffraction peaks related to C2MS phase with high intensity. As has been reported by Jiang et al. [28] C2MS phase occurs in co-precipitation process only when the molar content of the calcium precursor is double of the magnesium precursor in the reaction mixture. However, we found that the composition of obtained product depends strongly upon the solvent composition. The solubility product (k_{sp}) value of the intermediate hydroxide state of the final material depends strongly on the dielectric constant of the solvent; and a decrease of solvent dielectric constant reduces the k_{sp} value of the hydroxide. As water has higher dielectric constant (ε_w=79.5) than ethanol (ε_E=24.9), [30] Ca precipitates faster in water than in ethanol. Therefore, we obtained the final product with high content of calcium i.e. C2MS phase when the water as a solvent.

Fig. 2 shows typical TEM images of the samples synthesized using different volume ratios of water and ethanol. All the samples were calcined at 1100 °C for 2 h in air. Formation of well dispersed nanoparticles from 5 to 20 nm sizes in the samples is clear from the TEM micrographs.

Fig. 3 shows the energy dispersive analysis of X-ray (EDAX) spectra for the CMS samples synthesized with different water and ethanol ratios. The EDAX spectra revealed the presence of Eu in all the samples along with the emissions correspond to Ca, Mg, Si, O and Eu. Elemental compositions of all samples in atomic percentage are given in the Table 1. The amount of Ca in the samples increased with the increase of water content in the solvent, as predicted from our XRD results.

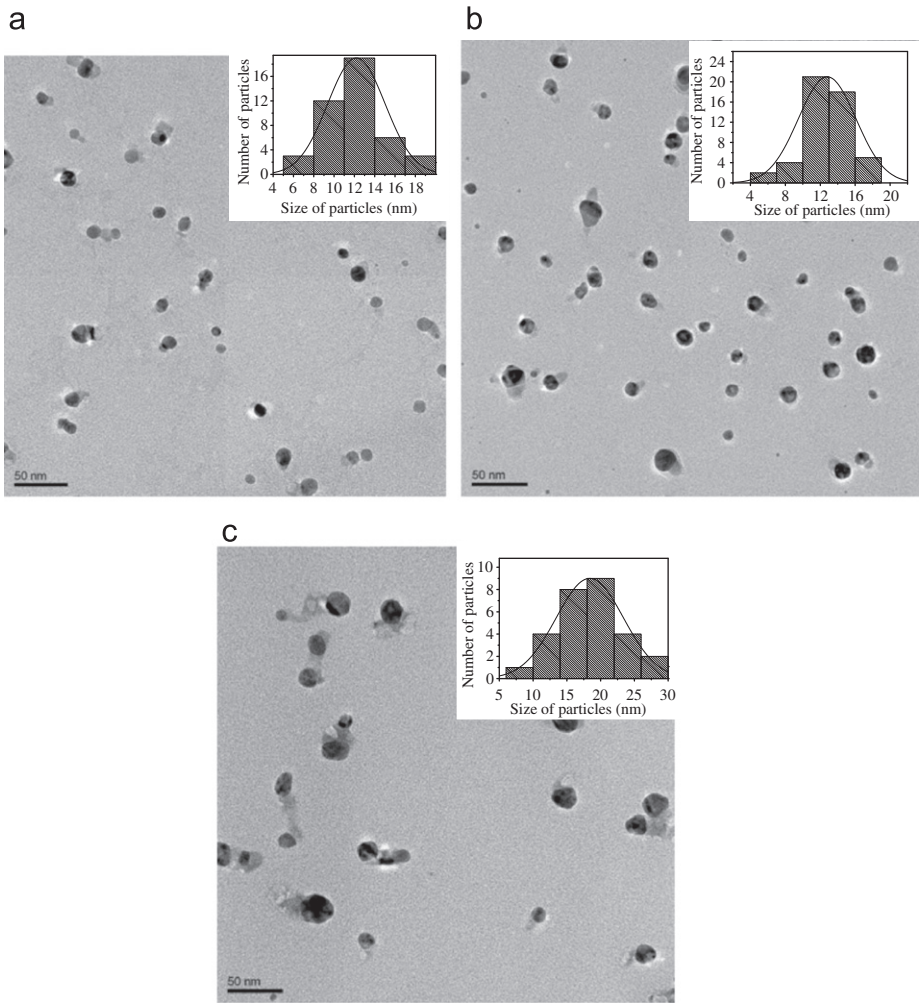

Fig. 2. Typical TEM images of the CMS nanophosphors prepared using water–ethanol volume ratio (A) 0:1, (B) 1:1 and (C) 1:0. Particle size distribution histograms for the samples are presented as insets of the corresponding TEM images.

XPS survey spectra of the samples synthesized with different water–ethanol volume ratios are shown in the Fig. 4. All the spectra were corrected for instrument and sample charges considering the C 1s position at 284.6 eV. All the samples revealed photoelectron peaks correspond to Ca 2p, Mg 2p, Si 2p, O1s, C1s and Eu3*d*5 emissions. The high resolution XPS spectra at Eu3*d*5 emission position for the samples synthesized with different volume ratios of water and ethanol are shown in Fig. 5. Presence of Eu activator in both Eu^{2+} and Eu^{3+} oxidation states in the samples is clear from their high resolution XPS spectra (Fig. 5). [31–33]. The intensity ratio $Eu^{3+}/(Eu^{3+}+Eu^{2+})$ decreased with the increase of water–ethanol volume ratio in the reaction solvent (inset of Fig. 5). As Ca^{2+} in CMS has lattice sites with six-fold oxygen co-ordination [28], when Eu^{3+} ions are incorporated into the CMS lattice, Eu^{3+} would replace Ca^{2+} site, since the radius of Eu^{3+} is (r=0.107 nm) [34] similar to that of Ca^{2+} (r=0.1 nm). However, due to unsatisfactory charge balance and high thermal energy of formation (calcination at high temperature), weak oxygen bond of Eu_2O_3 (i.e. single oxygen bond with europium in Eu_2O_3) breaks to proportionate one electron to trivalent europium, converting a fraction of Eu^{3+} into Eu^{2+}. The phenomenon can be presented through Krőger-Vink notation, generally used to describe the lattice position and electric charge of point defect species in crystals. In the Krőger-Vink notation M_s^c'M' denotes the nature of species, 's' is occupied species, and 'c' indicates charge or the ionization state ('x' for null charge, 'e' for an electron and '•' for positive charge). The electronic charge transfer between the ionized activators in CMS host lattice in the present case can be expressed as:

$$\tfrac{1}{2}(Eu_2O_3)+MgO+2SiO_2 \rightarrow Eu_{Ca}^{\bullet}+Mg_{Mg}^{x}+2Si_{si}^{x}+e+\tfrac{1}{2}O_2(g). \quad (1a)$$

ESR measurement was performed to examine the valence state of europium ions in the synthesized materials. The ESR spectra of the samples prepared using solvents of different water–ethanol volume ratios are presented in Fig. 6. Fig. 7 shows the electronic configuration of europium atom, Eu^{2+} and Eu^{3+} ions. As can be seen in the case of europium atom, 'f' subshell is half-filled, so

Total orbital quantum number L=0,
Spin quantum number S=7/2,
and angular momentum quantum number $J=S$=7/2.

Hence ground state term is $^8S_{7/2}$. In the formation of Eu^{2+} state, two electron from '6s' shell lost so '6s' shell becomes empty and 'f' subshell is half-filled therefore ground state term of Eu^{2+} is similar to Eu atom i.e. $^8S_{7/2}$.

In the case of Eu^{3+} ion formation, two electron from '6s' shell and one electron from '4f' shell lost so L=3, S=3 and J=0 ($J=L-S$, if less than half-filled of the subshell is occupied by electrons) hence ground state term is $^7F_0$. In Eu^{2+} ion number of free electrons are 7, out of that 6 can form three pairs of electrons and it will have one unpaired electron; while Eu^{3+} ion containing

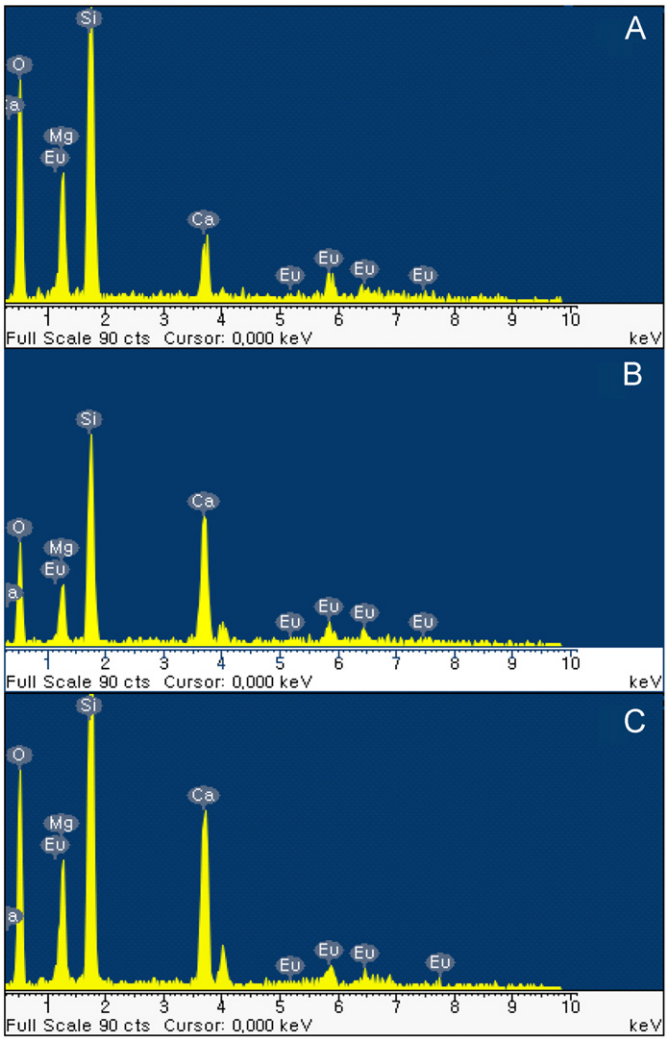

Fig. 3. Typical EDAX spectra of the CMS nanophosphors prepared using water–ethanol volume ratio (A) 0:1, (B) 1:1 and (C) 1:0. All samples were calcinated at 1100 °C for 2 h in air.

Table 1
EDAX elemental composition of the Eu doped CMS nanoparticles synthesized with different volume ratios of water and ethanol.

Water: Ethanol (W:E)	Atom (%)				
	O	Si	Mg	Ca	Eu
0:1	68.63	18.52	8.71	2.85	1.28
1:1	68.86	15.37	7.32	7.56	0.89
1:0	64.38	16.94	7.10	10.08	1.50

six free electrons, get coupled to form three pairs of electrons, does not have any unpaired electron. Due to the presence of unpaired electron in Eu^{2+}, X-band ESR spectra revealed a broad band powder patterned singlet signals, characteristic of Eu^{2+}. The powder patternedbroad singlet ESR bands with $g=2.2737$ and 4.2873 in the Fig. 6 clearly revealed the presence of Eu^{2+} state in the synthesized samples. As has been stated earlier, in the sample prepared using pure water as solvent (curve A of the Fig. 6) there exist two phases (CMS and C2MS). In the case of C2MS, Eu^{2+} ions occupy two different kinds of lattice sites with coordination number of six and eight; whereas, in CMS, Eu^{2+} ions occupy only one kind of lattice site with coordination number six [28]. Most probably the peaks with g values 2.2737 and 4.2873 observed for

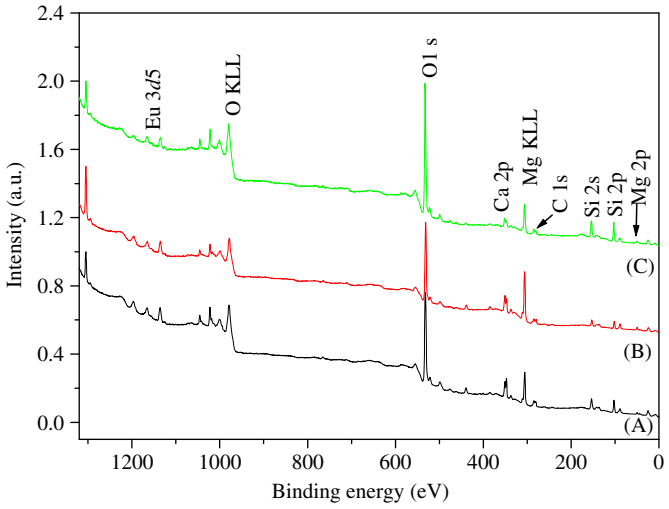

Fig. 4. XPS survey spectra of the CMS samples prepared with water–ethanol volume ratio (A) 0:1, (B) 1:1 and (C) 1:0. All samples were calcinated at 1100 °C for 2 h in air.

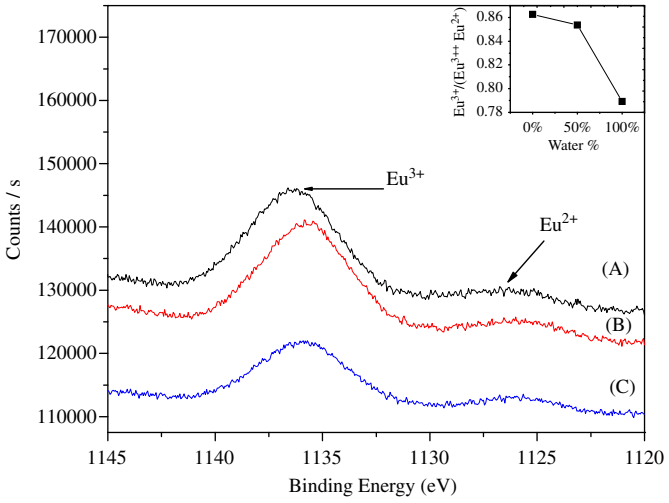

Fig. 5. High resolution XPS spectra at Eu3*d*5 position of the nanophosphors prepared with water–ethanol volume ratio (A) 0:1, (B) 1:1 and (C) 1:0. Variation of intensity ratio $Eu^{3+}/(Eu^{2+}+Eu^{3+})$ with the variation of water content in the reaction solvent is presented as inset.

the sample prepared with pure water as solvent (curve A, Fig. 6) are possibly related to the coordination number six and eight of the Eu^{2+} sites, respectively. Malchukova and Boizot has reported that Eu in ABS (aluminoborosilicate) glass can produce different Eu^{2+} sites with different coordination numbers and it will show separate g value of each coordination number [35]. This peak with $g=4.2873$ is absent in other two samples (W:E=1:1 and 0:1) where no C2MS phase was formed. However, presence of the activator in Eu^{2+} oxidation state in all the synthesized samples is evident from their ESR spectra. Presence of europium in Eu^{2+} state in high temperature air annealed CMS crystals has also been observed by Im et al. [33], which was associated to the rigid structure of CMS, acting as oxidation shield.

Fig. 8 shows the energy level diagram of Eu^{3+} and Eu^{2+} state of europium atom. In Eu^{3+} state, excitation wavelength is 395 nm, that means electron excitation as $^7F_0 \rightarrow {}^5D_4$. This excited electron get relax from $^5D_4 \rightarrow {}^5D_0$ without photoemission. Electronic transition takes place between $^5D_0 \rightarrow {}^7F_1$ with emission at 615 nm wavelength. In Eu^{2+} state electron excited from $^8S_{7/2}$ ground state to $4f^65d$ excited state at 337 nm wavelength and get

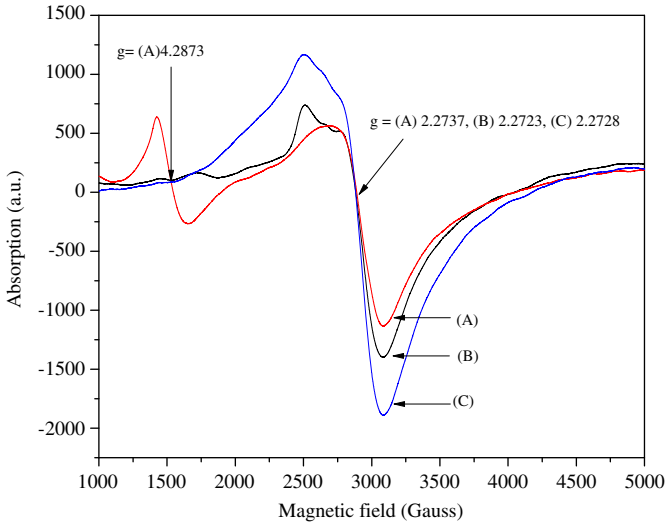

Fig. 6. ESR spectra of the CMS nanophosphors prepared with water–ethanol volume ratio (A) 0:1, (B) 1:1 and (C) 1:0. All the samples were calcinated at 1100 °C for 2 h in air.

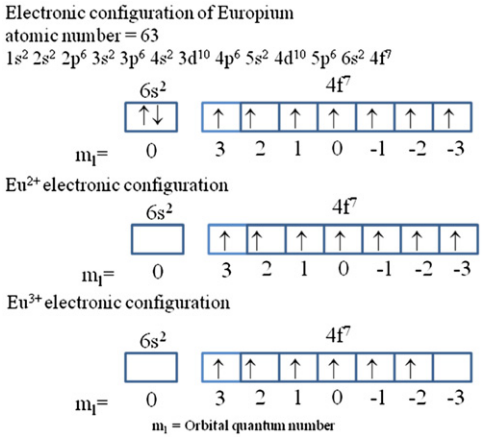

Fig. 7. The electronic configuration of Europium atom, Eu^{2+} and Eu^{3+} ions.

relax from $4f^6 5d \rightarrow 4f^6 5d^*$. This relaxed electron de-excite as $4f^6 5d^* \rightarrow {}^8S_{7/2}$ with blue emission at 450 nm wavelength. Photoluminescence (PL) spectra were recorded at room temperature under excitations at 337 and 395 nm to study the blue and red emissions in the nanophosphors. Comparative PL spectra of the synthesized samples in the blue and red emission regions are presented in the Figs. 9 and 10, respectively. Blue and red emissions of the nanophosphors appeared at about 451 and 615 nm, respectively. These two main emissions correspond to the Eu^{2+} and Eu^{3+} ionization states of the incorporated activator in the host matrix. The radius of Eu^{3+} is (r=0.107 nm) similar to that of Ca^{2+} (r=0.1 nm). So when Ca^{2+} is replaced by Eu^{3+} red emission take place, but due to unsatisfactory charge balance and high thermal energy exchange (calcination at high temperature), a fraction of Eu^{3+} converted into Eu^{2+}. When these Eu^{2+} ions exchange Ca^{2+} ions, blue emission take place. The blue emission (Fig. 9) arises due to the transition between the 5d excited and $4f^7$ ground state energy level of Eu^{2+} [29], while the red emission (Fig. 10) corresponds to the ${}^5D_0 \rightarrow {}^7F_2$ transition [36,37] of Eu^{3+} ions. The other two weak shoulder peaks appeared at about 590 and 630 nm in this region correspond to the ${}^5D_0 \rightarrow {}^7F_1$ and ${}^5D_0 \rightarrow {}^7F_3$ transitions, respectively [38]. Intensity of the blue emission (451 nm) decreased drastically with the increase of water content in the solvent. Variation of intensity ratio between

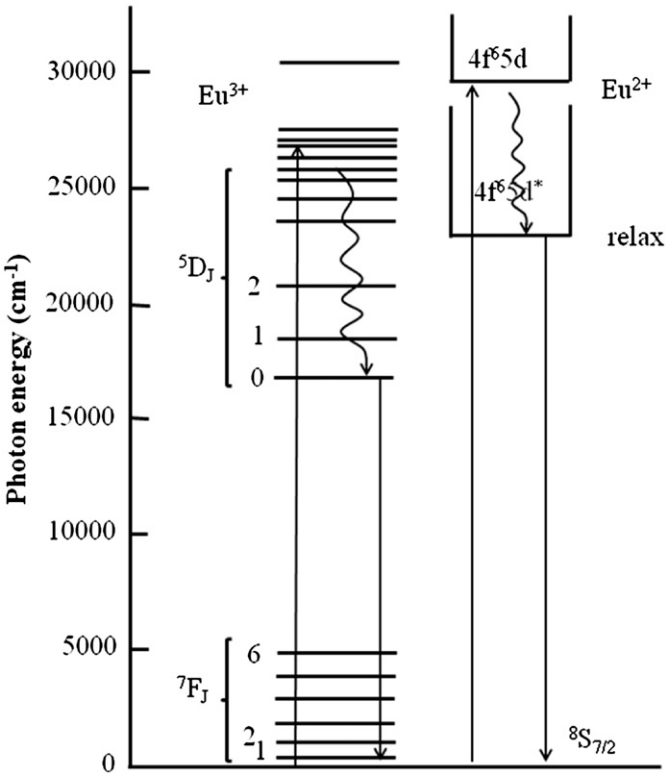

Fig. 8. Energy level diagram of Eu^{3+} and Eu^{2+} state of Europium atom.

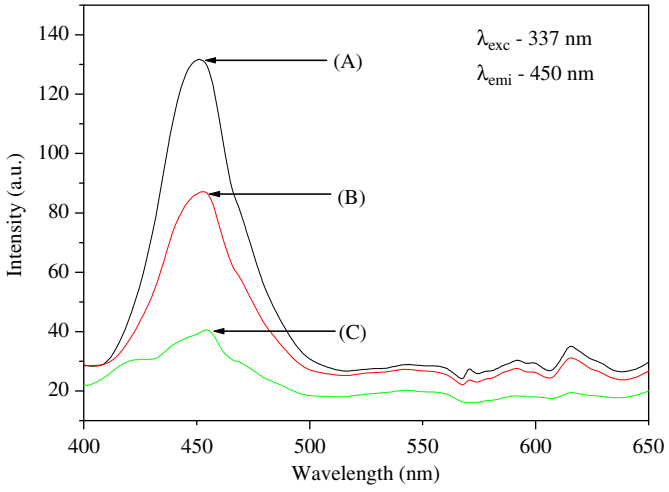

Fig. 9. Room temperature PL spectra in the blue emission region for the nanophosphors prepared using water–ethanol volume ratio (A) 0:1, (B) 1:1 and (C) 1:0. All samples were calcinated at 1100 °C for 2 h in air.

the emission band corresponds to Eu^{3+} ions and the integral emission (correspond to Eu^{3+} and Eu^{2+} ions) on the variation of water content in the solvent is plotted as the inset of Fig. 10. As can be noticed, the relative emission intensity correspond to Eu^{3+} ions decreases with increasing the volume fraction of water in the solvent, in accordance with the variation of corresponding ion concentrations estimated from their XPS studies (inset of Fig. 5).

Cathodoluminescence spectra of CMS nanophosphors synthesized using different solvent ratios of water and ethanol is shown in Fig. 11. The spectra show blue light at 460 nm and red light at 630 nm. The intensities of blue and red light were found to be increased with increasing concentration of ethanol in solvent ratio. This is because with increasing the concentration of ethanol

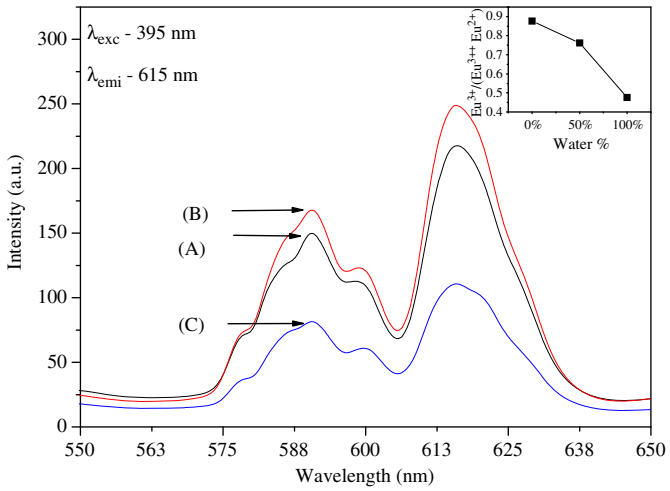

Fig. 10. Room temperature PL spectra in the red emission region for the nanophosphors prepared using water–ethanol volume ratio (A) 0:1, (B) 1:1 and (C) 1:0. All samples were calcinated at 1100 °C for 2 h in air. Variation of $I^{3+}_{Eu}/(I^{2+}_{Eu}+I^{3+}_{Eu})$ with the variation of water content in the solvent is presented as inset.

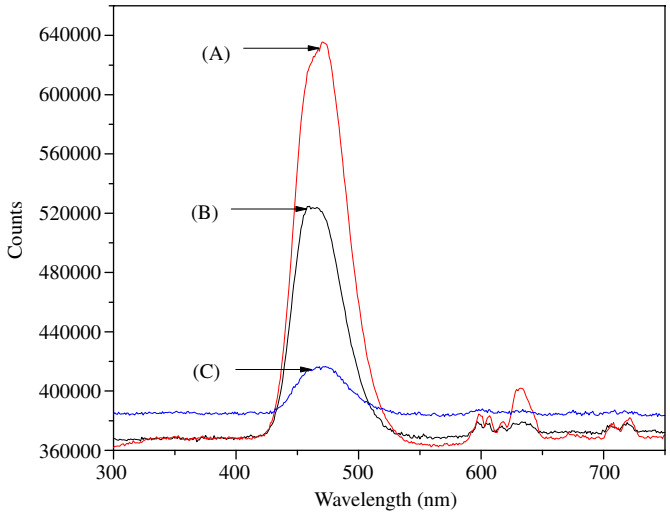

Fig. 11. Cathodoluminescence (CL) spectra of the CMS nanophosphors prepared using water–ethanol volume ratio (A) 0:1, (B) 1:1 and (C) 1:0.

pure CMS phase formation takes place, which was already discussed in XRD spectra. In the case of CL, when high energy electron beam incident on the sample, number of signals generated such as X-rays, secondary electrons, backscattered electrons, auger electrons, phonons and photons [39]. For CL, detector detect only photons signal generated from the sample. The spectra show large variation in the intensity of blue and red emission. The difference in emission intensity can relate to absorption of low energy red light by the phonon i.e. lattice vibration of material. We also observed red shift in blue as well as red emission by 10 and 15 nm, respectively, from the emission peaks observed in PL spectra (Figs. 9 and 10). This is because the trap energy level between valence band and conduction band shifts towards valence band as the material gets heated during CL analysis.

As the water content in the solvent plays vital roles in controlling the particle size, activator concentration (i.e. Eu concentration), and ionization state of the activator in the CMS nanophosphors, by changing the composition of the reacting medium (solvent) their blue and red emission efficiencies could be controlled.

4. Conclusion

Spherical CMS nanoparticles of size ranging from 5 to 20 nm could be successfully synthesized using the room temperature co-precipitation technique. Composition of the reaction medium/solvent, and hence its effective dielectric constant plays important roles in controlling the particle size, composition, and dopant incorporation in the nanophosphors. Particle size of the nanophosphors decreases with the decrease in dielectric constant of solvent. Water fraction in the water–ethanol mixed solvent also controls the ionization state of the activator/dopant, thereby controlling the blue and red emission efficiencies of the nanophosphors.

Acknowledgments

This work was supported by Basic Research Program through the National Research Foundation of Korea (NRF) grant funded from the Ministry of Education, Science and Technology (MEST) of Korea for the Center for Next Generation Dye-Sensitized Solar Cells) (no. 2010-0001842).

References

[1] M.Y. William, S. Shigeo, Y. Hajime, Phosphor Handbook, Second Ed, CRC Press, New York, 1998.
[2] K.Y. Jung, J.H. Kim, Y.C. Kang, J. Lumin. 129 (2009) 615.
[3] L. Jiang, C. Chang, D. Mao, C. Feng, J. Alloys Compd. 377 (2004) 211.
[4] Y. Kim, L.C. Ming, M.H. Manghnani, Earth Planet. Inter. 83 (1994) 67.
[5] K. Oguri, N. Funamori, F. Sakai, T. Kondo, T. Uchida, T. Yagi, Phys. Earth Planet. Inter. 104 (1997) 363.
[6] T. Irifune, M. Miyashita, T. Inoue, J. Ando, K. Funakoshi, W. Utsumi, Geophys. Res. Lett. 27 (2000) 3541.
[7] S. Nakajima, Y. Harada, Y. Kurihara, T. Wakatsuki, H. Noma, Shikwa Gakuho 89 (1989) 1709.
[8] T. Nonami, Mater. Res. Soc. Symp. Proc. 252 (1992) 87.
[9] N.Y. Iwata, G.H. Lee, S. Tsunakawa, Y. Tokuoka, N. Kawashima, Colloids Surf., B 33 (2004) 1.
[10] T. Kunimoto, R. Yoshimatsu, K. Ohmi, S. Tanaka, H. Kobayashi, IEICE Trans. Electron 11 (2002) 1888.
[11] K.Y. Jung, K.H. Hana, Y.C. Kang, H.K. Jung, Mater. Chem. Phys. 98 (2006) 330.
[12] S. Nakajima, Shikwa Gakuho 90 (1990) 525.
[13] T. Nonami, Mater. Res. Soc. Symp. Proc. 175 (1990) 71.
[14] G.R. Fleming, G. Scholes, Nature 431 (2004) 256.
[15] C. Roger, M.G. Muller, M. Lysetska, Y. Miloslavina, A.R. Holzwarth, F. Wurthner, J. Am. Chem. Soc. 128 (2006) 6542.
[16] J.W. Verhoeven, J. Photochem. Photobiol. C 7 (2006) 40.
[17] P. Cosma, F. Longobardi, A. Agostiano, J. Electroanal. Chem. 564 (2004) 35.
[18] J.J. Griffin, T.G. Ranney, D.M. Pharr, J. Am. Soc. Hortic. Sci. 129 (2004) 46.
[19] S. Lian, C. Rong, D. Yin, S. Liu, J. Phys. Chem. C. 113 (2009) 6298.
[20] B. Yan, W. Wang, Y. Song, Spectrochim. Acta A 66 (2007) 1115.
[21] T.A. Fayed, M.K. Awad, Chem. Phys. 303 (2004) 317.
[22] A.S. Klymchenko, Y. Mely, Tetrahedron Lett. 45 (2004) 8391.
[23] D.H. Pan, D.H. Hu, R.C. Liu, X.H. Zeng, S. Kaplan, H.P. Lu, J. Phys. Chem. C 11 (2007) 8948.
[24] N. Pradhan, D. Goorskey, J. Thessing, X. Peng, J. Am. Chem. Soc. 127 (2005) 17586.
[25] S. Comby, R. Scopelliti, D. Imbert, L. Charbonnie're, R. Ziessel, J.C.G. Bu1nzli, Inorg. Chem. 45 (2006) 3158.
[26] T.J. Chow, S.H. Tsai, C.W. Chiu, T.S. Yeh, Synth. Met. 149 (2005) 59.
[27] A. Ajayaghosh, C. Vijayakumar, V. Praveen, S.S. Babu, R. Varghese, J. Am. Chem. Soc. 128 (2006) 7174.
[28] L. Jiang, C. Chang, D. Mao, J. Alloys Compd. 360 (2003) 193.
[29] A. Daud, T. Kunimoto, R. Yoshimatsu, K. Ohmi, S. Tanaka, H. Kobayashi, ICSE2000 Proceedings, Nov. 2000.
[30] S.M. Puranik, A.C. Kumbharkhane, S.C. Mehrotra, J. Mol. Liq. 59 (1994) 173.
[31] W.D. Schneider, C. Laubschat, I. Nowik, G. Kaindl, Phys. Rev. B 24 (9) (1981) 5422.
[32] S. Han, S.J. Oh, J.H. Park, H.L. Park, J. Appl. Phys. 73 (9) (1993) 4546.
[33] W.B. Im, J.H. Kang, D.C. Lee, S. Lee, D.Y. Jeon, Y.C. Kang, K.Y. Jung, Solid State Commun. 133 (2005) 197.
[34] D.R. Lide, H.P.R. Frederikse, CRC Handbook of Chemistry and Physics, 77th edn, CRC Press, Boca Raton, 1996, pp. 12–14.
[35] E. Malchukova, B. Boizot, Mater. Res. Bull. 45 (2010) 1299.
[36] A.P. Jadhav, A.U. Pawar, C.W. Kim, H.G. Cha, U. Pal, Y.S. Kang, J. Phys. Chem. C 113 (2009) 13600.
[37] Q. Li, L. Gao, D.S. Yan, Wuji Cailiao Xuebao 12 (2) (1997) 237.
[38] P.Y. Jia, J. Lin, X.M. Han, Thin Solid Films 483 (2005) 122.
[39] S. Boggs, D. Krinsley, Application of Cathodoluminescence Imaging to the Study of Sedimentary Rocks, Cambridge University Press, 2006.